Bone Reposition Planning for Corrective Surgery Using Statistical Shape Model: Assessment of Differential Geometrical Features

Neda Sepasian[1], Martijn Van de Giessen[2], Iwan Dobbe[3], and Geert Streekstra[3]

[1] Department of Biomedical Image Analysis, TU/e, Eindhoven, The Netherlands
[2] Division of Image Processing, LUMC, Leiden, The Netherlands,
[3] Department of Biomedical Engineering and Physics, AMC, Amsterdam, The Netherlands

Abstract. We discuss a new planning method for corrective osteotomy surgery without the need to make a CT scan of the contralateral bone. We use a statistical shape model to estimate the most likely relative position of two bone segments of an osteotomized bone. To investigate the added value of geometrical properties for planning, different geometrical features of the bone surface are being incorporated. The feasibility and accuracy of our proposed method are investigated using 10 virtually deformed radii and a statistical shape model based on 35 healthy radii.

1 Introduction

Limb fractures are very common and sometimes result in malunion of the fractured bone segments causing chronic pain, reduced function and finally osteoarthritis. For the distal radius, e.g., the annual incidence rate is approximately 0.3% of the population each year [1], while about 5% of these cases result in a symptomatic malunion requiring secondary treatment by corrective osteotomy surgery [2]. In this procedure the bone is cut in two segments which are repositioned and fixated, mostly using an anatomical plate and screws.

In state-of-the-art techniques for planning of such a surgical reconstruction virtual 3-D bone models are created from CT volume data of the affected bone. In this approach the CT data of the mirrored contralateral limb is used as a reconstruction target in the planning procedure. [3–6]. A drawback of this approach is that a healthy contralateral reference is not always available. Also, this standard approach requires a CT scan of the healthy limb as well, which increases the radiation dose by a factor of two.

To overcome these drawbacks a method is required that can provide the planning of the surgical reconstruction based on the affected bone only by using shape information of the unaffected segments of the bone. For such a planning method application of a statistical shape model (SSM) of the bone [7, 8] fitted to the surface data of the unaffected bone parts seems a logical choice which allows prediction of the optimal alignment of the bone segments after surgery. In this context the SSM model describes the patterns that exist within the variation in shape in a population [9].

M.J. Cardoso et al. (Eds.): BAMBI 2014, LNCS 8677, pp. 49–60, 2014.

Recently SSM's were reported to be advantageous in a large number of orthopedic applications such as robust and fast bone segmentation [10, 11], creation of bone geometries for finite element modeling [12, 13], implant design optimization [14, 15] and several diagnostic applications [9, 16]. Related to our problem SSM's have been used to reconstruct bone surfaces from incomplete bone geometry representations for surgical planning and navigation [17]. In this paper we make an essential additional step by incorporating the alignment of the bone segments in the fitting procedure of the SSM to the incomplete bone surface data.

The general framework concerning the surface fitting problem use deviations in surface geometry between a reference shape and a target shape to fit one single shape to the other [18, 19]. The classic method for surface fitting is based on the iterative closest point (ICP) algorithm. This method minimizes the distance between points in one surface and the closest points in another surface [20, 21]. A surface matching algorithm was also developed for fitting a statistical shape model (SSM) of a same type of surface to a target surface [22]. In these methods, random point sets on a surface are being identified and these point clouds are registered and matched to compute the corresponding points.

A common way to control surface fitting is to use distance information between the reference and target during optimization, e.g., using Euclidean norms. This choice however exploits only limited information about the surface geometry. It is possible however, to add additional geometrical features such as different shape related vector fields and curvature as ingredients in controlling the fit. To this end, different approaches have been developed for matching source and target surface invariants such as curvature maps [19, 23]. All these methods require the iteratively updating of corresponding points during the fitting procedure which is a time consuming step. Furthermore, it is known that including the corresponding points results in a convergence to local minima due to the partial alignment instead of the global minimum indicating the perfect alignment.

In this paper we propose a method for surface-fitting of a SSM to the geometrical representation of an affected bone to plan realignment of two bone segments during corrective surgery. Moreover, we investigate the efficiency of using different metrics for fitting the SSM to the segments of a target bone. To this end we optimize the fitting of the model to the target bone using individual features such as spatial distances, curvature and curvature vectors. Primarily, our goal is to develop a method which does not require the availability of corresponding points, nor the data set of the contralateral bone. However, this requirement becomes essential in the presence of the curvature and curvature vectors. To this end, we propose a cost function that can be customized for this purpose. The residual positioning error for different optimization metrics is examined experimentally, using virtual malunions of radii outside those used for building the SSM.

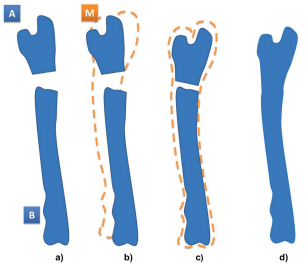

Fig. 1. Sketch for illustrating the correction prototype, a) Initial bone segment positions, b) Initial bone position M c) Intermediate step where the model is deformed, scaled and translated and bone segment A has been translated and rotated, d) the final model where the most likely solution has been found

2 SSM Based Planning

The challenge is to find the correct relative position of the distal and proximal bone segments from a single malunited bone. The surfaces A and B of both bone segments are initially sub-optimally aligned due to the malunion; see Figure 1.a. To find the correct alignment of these bone segments we propose to fit a statistical shape model M built from multiple segmentations of bones to patient data containing the two segments A and B of the bone. For initialization we use the statistical model M close to the two bone segments (Figure 1.b). Subsequently, an iterative optimization process is performed in which A is subject to translations and rotations, B is considered fixed, and M is translated, rotated, scaled and reshaped until A and B optimally fit with M. After convergence the translation and rotation parameters of A with respect to B describe the repositioning parameters that needs to be applied to A during surgery (Figure 1.c). The best-fitting shape M describes the most likely shape of the original bone (Figure 1.d).

An extra-articular fracture resulting in a malunion often shows a deformed region between a distal (A) and proximal (B) bone segment. In a malunion the distal bone segment is malpositioned with respect to the proximal bone segment, but apart from the location of malunion, the shapes of these bone segments are unaffected. Since the deformed region is unlike normal bone geometry we exclude it from the fitting procedure in our planning method.

2.1 Fitting of the SSM to Two Bone Segements

During the fitting process bone segment A and the model M are subject to translation t_A and t_M and rotation r_A and r_M computed by three Rodrigues rotation parameters. The model M is also allowed to scale indicated by the parameter s_M and to distort using the shape parameter $\boldsymbol{b}$. The variables to be optimized are $\boldsymbol{R} = [r_A; t_A; r_M; t_M; s_M; \boldsymbol{b}] = [\boldsymbol{R}_A; \boldsymbol{R}_M; \boldsymbol{b}]$.

The total likelihood to correct the two bone parts A and B orientation and position with respect to each other using a model M consists of the shape similarity, scaling and feature measures and reads

$$L(A, B, M, \boldsymbol{R}) = P_f(B \cup A(\boldsymbol{R}_A) \mid M(\boldsymbol{R}_M)) + P_s(s_M) + P_b(\boldsymbol{b}). \quad (1)$$

where $P(\boldsymbol{b})$ is a probability density function representing the validity of a shape with shape parameter $\boldsymbol{b}$, $P(s_M)$ is a probability function for scaling and $P_f(X \mid M)$ is a probability density function for measuring the similarity between the statistical model M and bone surface X. For our particular application we have $X = B \cup A(\boldsymbol{R}_A)$. The probability density function V includes the representation of surfaces geometrical features, shape deformation and the closet neighborhood distance measure.

The optimal composition of bone parts A and B can then be obtained by maximizing $L(A, B, M, \boldsymbol{R})$. However, due to very low likelihood values in $P_f(B \cup A(\boldsymbol{R}_A) \mid M(\boldsymbol{R}_M))$, this might lead to numerical problems. Therefore we minimize the negative logarithm $-\log P_f(B \cup A(\boldsymbol{R}_A) \mid M(\boldsymbol{R}_M))$ using a standard gradient descent method. In the following, building of the SSM as well as each of the probability density functions are described in detail.

2.2 Probability Distribution Functions for Shape Validity and Scaling

In order to construct the SSMs in this paper the active shape modelling introduced in [7] has been applied. We represent each bone by a $3n$ element vector formed by concatenating the elements of the individual surface points $\boldsymbol{x}_i = [x_1, y_1, z_1, \cdots, x_n, y_n, z_n]$, $i = 1, 2, \cdots, l$ where l is the number of individual shapes. Formally, each shape can be described using the linear model

$$\boldsymbol{x} = \boldsymbol{m} + \boldsymbol{P}\boldsymbol{b}. \quad (2)$$

Here, $\boldsymbol{m}$ consists of the coordinates of the mean shape, $\boldsymbol{P}$ is a matrix with modes of variation and $\boldsymbol{b}$ is a vector with the weighting parameters for the variations specified for each mode j. The non-rigid registration introduced in [24] has been applied in order to estimate the corresponding points of all shapes and consequently the mean $\boldsymbol{m}$ and the modes of variation $\boldsymbol{P}$ [7]. Using the weighted summation of the different modes of variations, a new shape can be computed.

The probability distribution function for scaling $P_s(s_M)$ is modeled using a 1D normal distribution with mean 1 and standard deviation s_M computed from the volume estimation during the SSM construction.

2.3 Probability Distribution Model to Compare Shapes

We propose a probability distribution function inspired by the registration model introduced in Granger *et al.* [25]. In this model the alignment of two point clouds

is being treated as a probability density maximization problem, where one point clouds is representing the centroid of a Gaussian Mixture Model (GMM) and the other one represents the data points. Ideally, two point sets become aligned and the correspondence is estimated using the Mahalanobis distance. Here, bone segment A are described by points a_j on the surface of A and points m_k are located on the surface of the deformed and transformed model M is described by a GMM. We propose a probability distribution which combines the point-wise distance (e.g. Euclidean) between the model and the patient data, the point-wise angle between any vector data corresponding to the point cloud shapes, and the differences in their curvature maps. Given the points $a_j; j = 1; 2; \cdots; n_A$ on A with n_A as the number of points in cloud A, then the likelihood that the point m_k in M is sampled as point on A is computed by

$$P(a_j \mid m_k) = \frac{1}{(2\pi)^{9/2}\left(\mid \Sigma_p \mid\mid \Upsilon_p \mid\mid \Gamma_p \mid\right)^{3/2}} \tag{3}$$
$$\exp(-\frac{1}{2}(\boldsymbol{d}_{jk}^{\top}\Sigma_p^{-1}\boldsymbol{d}_{jk})) + \exp(-\frac{1}{2}(\boldsymbol{c}_{jk}^{\top}\Upsilon_p^{-1}\boldsymbol{c}_{jk})) + \exp(-\frac{1}{2}(\boldsymbol{t}_{jk}^{\top}\Gamma_p^{-1}\boldsymbol{t}_{jk}))$$

Where the covariance matrix $\Sigma_p = \sigma_p I$ is a diagonal 3×3 matrix with the standard deviation σ_p and the identity matrix I. Respectively, $\Upsilon_p = \epsilon_p I$ and $\Gamma_p = \gamma_p I$ describe the different Covariance matrices for curvature and the vectors. In this work all n_M points of m_k; $k = 1; 2; \cdots; n_M$ in M are considered equally uncertain and therefore standard deviations are the same for all m_k. The Euclidean distance is $d_{jk}(a_j, m_k) = d_{jk} = \sqrt{\sum_{i=1}^{3}(a_j^i - m_k^i)}$ and the vector match measure is $t_{jk}(a_j, m_k) = t_{jk} = 1 - w(a_j, m_k)$. Where, $w(a_j, m_k) = v_j.v_k/|v_j|.|v_k|$, $0 \leq w \leq 1$ and v_j is the vector at point a_j where $|.|$ denotes the norm of the vector. The smaller is the angle between vectors at two points, the larger is the similarity between two point data. The vectors denote the principal curvature vectors. Later on in Section 5 we will clarify the principal curvature vector definition. Here, $c_{jk} = c(a_j, m_k)$ represents the difference between the curvature at a_j and m_k. Our probability function is customized in order to include the corresponding points. This setting possible as long as the nature of distribution of all the features can be well defined.

Given the statistical model (3), the likelihood $P(X \mid M)$ that all points in X are sampled from M is estimated by

$$P_f(X \mid M) = \sum_{j=1}^{n_A} P(a_j \mid M) = \sum_{j=1}^{n_A} \frac{1}{n_M} \sum_{k=1}^{n_M} P(a_j \mid m_k). \tag{4}$$

Where X is one or more bone segments.

3 Experiments

3.1 Data

The proposed method was evaluated using CT scans of healthy radii. To this end 45 radii (26 women, 19 men, age [11, 56] years) were imaged with voxel size

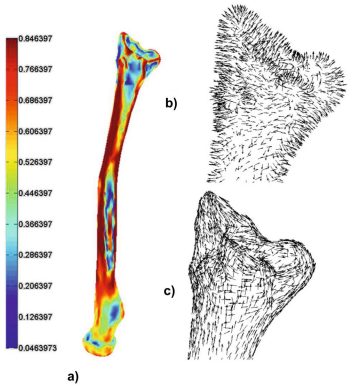

Fig. 2. a) Gaussian curvature map, the color bar indicates the maximum principal curvature, b) Normal vector illustration, c) maximum curvature vector

$(0.45 \times 0.45 \times 0.45)$mm using a Brilliance 64-channel CT scanner with a regular-dose, high-resolution protocol. In order to scan the complete radii individuals were scanned in prone position with the forearm extended above the head. Right radii polygons were created by image segmentation [4]. We mirror the cases where only the left radius was scanned. This resulted in 45 healthy right radii polygons. Ten of these were randomly selected as target bones, the remaining 35 bones were used as training shapes for building SSMs. Knowing the corresponding points of the bones inside the training set, enabled estimating σ, ϵ and γ using the standard deviation of the differences between the corresponding points distance-, curvature- and curvature vector-wise. Subsequent experiments were done using these values. In case more than one of these surface features was evaluated at the same time, linear combinations of the distance d_{jk}, curvature c_{jk} and tangent vector measure t_{jk} applied (3). We sampled 5000 points per surface. In the above-described experiment, optimization of the fitting procedure is based on the average nearest neighbor distance between points of the SSM and a target bone.

3.2 Evaluating the SSM

To investigate how many shapes are required to build a SSM that sufficiently represent a set of target bones, we randomly selected 10, 15, 20, 25 and 35 training shapes of complete bones to build the SSMs. This SSM was subsequently fit to the 10 target bones and the closet nearest neighbor distance was determined for each target bone, resulting in a mean and a standard deviation of this parameter. Figure 3.a shows the mean error and standard deviation values for these experiments. It is clearly shown that the mean and standard deviation reduce with the number of training shapes in the SSM. Our computations indicate the SSM containing 35 training shapes is considered sufficiently accurate to describe a target bone shape and is therefore used as SSM in the remainder of this document.

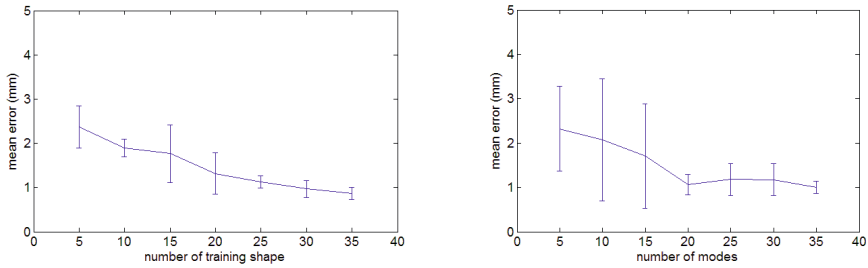

Fig. 3. a) Agreement between SSM and target bones as a function of the number of training shapes inside the SSM. b) Agreement between SSM, containing 35 training shapes, and target bones as a function of the number of modes of variation taken into account.

3.3 Evaluating Modes of Variation

The fitting procedure can be accelerated by only considering relevant modes of variation and disregarding higher modes of variation that merely represent noise. To evaluate how many modes of variation are required to fit the SSM with sufficient accuracy to a set of target bones, we performed fitting of the SSM to the 10 target bones taking into account an increasing number of modes of variation Fig. (3b). The nearest neighbor distance is again used to quantify the agreement between SSM and target bones. Based on this computations for the rest of the experiments we chose the first 25 modes of variations.

3.4 Including the Geometrical Features

We performed fitting of the SSM to the 10 target bones using different combinations of the geometrical features, 35 training shapes and 25 modes of variations. We estimating corresponding points based on minimum Euclidean distance. Figure 4 shows the computational result. Note that this figure only illustrates the result for the combination with more obvious variations with respect to the rest. We observe that including the geometrical features result in a more consistent fitting and smaller distribution of the standard deviation. This is due to the improvement of the local alignment. Using this computation for the repositioning experiment we choose the combination of distance and the curvature vector measure.

3.5 Accuracy of Bone Repositioning

To evaluate the accuracy of bone repositioning using the proposed method we simulated three virtual malunions for each of the 10 target bones, i.e., 30 simulated malunions. This enables comparing the reconstructed radius with its ground truth, i.e., the radius before the malunion. A malunion was simulated by

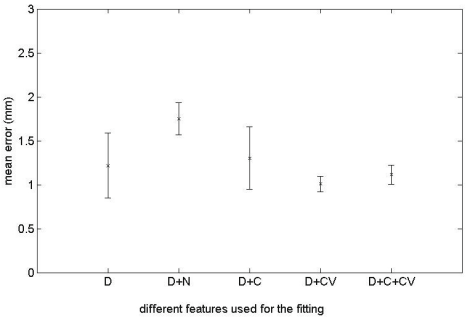

Fig. 4. Variation of the fitting using combination of different features using 35 training shapes and 25 modes of variations, D stands for distance, N is for normal vectors, C is for curvature, CV stands for curvature vectors.

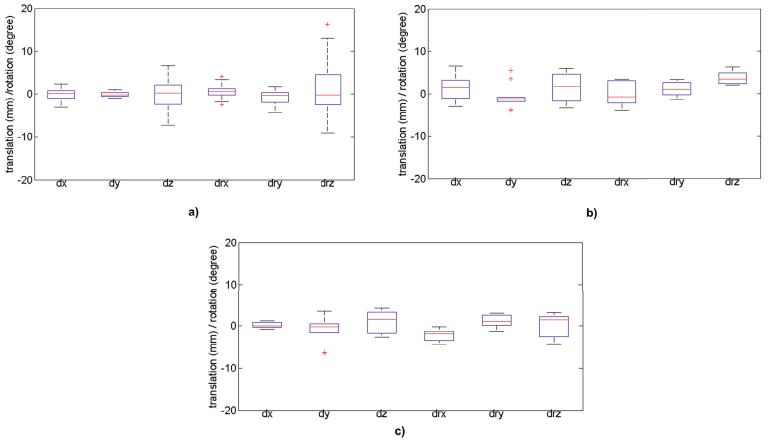

Fig. 5. Boxplot showing the accuracy of repositioning the distal radius segment with respect to the proximal segment, based on fitting a SSM to remaining bone segments in a simulation experiment (10 target bones, 3 deformities per bone). dx, dy and dz are translations between the centers of gravity of the reconstruction result and the ground truth. drx, dry and drz are the rotations about the x, y and z axes. a)reconstruction using bilateral asymmetry [26] b) reconstruction using distance measure. c) reconstruction using distance and curvature vectors.

removing a bone piece between a distal and proximal bone segment and by randomly translating (range $[2, 5]$mm) and rotating (range $[10, 60]^\circ$) the distal part. The height of the randomly removed piece (the defect) is called the defect height (range [3, 7] mm). The simulated bone was subsequently reconstructed using the proposed method. Figure 5 shows the residual rotation r_r and translation t_r error with respect to the ground truth as box plots. The box represents standard

deviation , the horizontal line the mean value and the whiskers represent the range. Figure 5.a indicates differences due to bilateral asymmetry reported by Vroemen et al. [26] as determined for 20 individuals by left-to-right matching and right-to-left matching of distal and proximal segments, explaining the different sign in their results. These dots enable comparing repositioning results of the proposed method with generally accepted variations since the contralateral side is normally considered the best reference available. Figure 5a shows the estimated error when only the probability distance measure is used as metric during the fitting procedure.

We observe the improvement of the error distribution level in comparison with the fit using bilateral differences. The translation errors dx, dy and dz are smaller than acceptable levels considering the bilateral differences. For rotation, also we see an improvement in comparison with the bilateral differences particularly about the z-axis, i.e., the longitudinal axis of the bone. In general, we observe a slight improvement by adding curvature geometrical features; see Figure 5b and 5c. Figure 6b is a typical example after reconstruction with only distance as optimization metric. Figure 6c − d shows the common reconstruction error which occurs by only using the distance measure. The experiments were performed for different defect heights and we noticed the larger error occurs with larger heights.

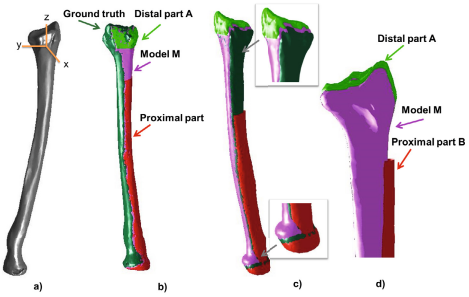

Fig. 6. a) Axes defined within the radius and heights of removals, b) correctly reconstructed bone, c) common translation and rotation error occurs using only the distance d) poorly reconstructed bone with 10 degrees rotation error about the z-axis and 4 mm translation error along the x-axis.

4 Discussion

We introduced a new technique for repositioning bone segments after a fracture or malunion using a SSM of the radius and a set of differential geometry features for surface-to-surface fitting. The method yields a set of transformation and rotation parameters, which can be used in a device for the actual bone repositioning; see [27]. We showed that residual positioning errors are very close to what can be achieved compared to standard 3-D planning, which is limited as a result of bilateral differences [26]. The use of only a distance measure as metric for the optimization of fitting seemed slightly inferior to using a metric that includes

the shapes curvature and/or curvature vectors, particularly, when a larger piece of the bone is removed.

Our study aimed at modeling the radius although it can be easily extended for other bone types as well. The presented method requires an initial segmentation step. In future studies this can be avoided by performing the fitting and obtaining the geometrical features directly using CT grayscale volumes. It reduces a possible observer bias and increases the degree of automation since no user interaction is required for segmentation.

A big advantage of the proposed method is the fact that a contralateral bone is not required. This allows bone repositioning when a contralateral bone is not available. In addition, it reduces the radiation-absorbed dose, since the contralateral arm does not need to be scanned. In this pilot study residual errors in repositioning parameters already appeared to be very close to what can be achieved compared to conventional 3-D planning based on bilateral symmetry, we expect that the method will show valuable in the next generation of planning applications.

5 Appendix

Let $x_i = x_i(u, v), i = 1, 2, 3$ be a regular parameterizations of a surface. The Gaussian curvature of a surface in R^3 is given by

$$k = \kappa_1 \kappa_2 = \frac{LN - M^2}{EG - F^2},$$

where κ_1 and κ_2 are the principal curvature, $E = x_u \cdot x_u, F = x_u \cdot x_v$ and $G = x_v \cdot x_v$ are coefficients of the first fundamental form and $L = x_{uu} \cdot n, N = x_{vv} \cdot n, M = x_{uv} \cdot n_i$, are coefficients of the second fundamental form. These coefficients are computed at given point x_i in the parametric plane by the projections of the second partial derivatives of x at that point onto the normal vector n. In this setting, it is easy to see why the Gaussian curvature is independent of the choice of the unit normal n. Notice that if the sign of n is reversed, the signs of the coefficients of L, M, N are reversed too. Further, while the signs of both principal curvatures κ_1 and κ_2, the product $K = \kappa_1 \kappa_2$ remains unaffected. Clearly, the sign of mean curvature $H = \frac{(\kappa_1 + \kappa_2)}{2}$, depends on the choice of sign of n. In order to compute the curvature vectors, we compute the terms of the first and second fundamental forms and define the corresponding metric tensors [28],

$$F_1 = \begin{bmatrix} E & F \\ F & G \end{bmatrix}, \quad F_2 = \begin{bmatrix} L & M \\ M & N \end{bmatrix}, \tag{5}$$

and we introduce

$$O = inv(F_1) F_2.$$

The previously introduced principal curvatures κ_1, κ_2 are the eigenvalues of the matrix O. The eigenvectors of the matrix O are corresponding to the vectors pointing to the direction of κ_1, κ_2 respectively (Figure 6a − c). Therefore, a shape can be described by the type of curvature and the type of the orientation.

References

1. Athwal, G.S., Ellis, R.E., Small, C.F., Pichora, D.R.: Computer-assisted distal radius osteotomy. The Journal of Hand Surgery 28(6), 951–958 (2003)
2. Miyake, J., Murase, T., Moritomo, H., Sugamoto, K., Yoshikawa, H.: Distal radius osteotomy with volar locking plates based on computer simulation. Clin. Ortho. and Rel. Res. 469(6), 1766–1773 (2011)
3. Cronier, P., Pietu, G., Dujardin, C., Bigorre, N., Ducellier, F., Gerard, R.: The concept of locking plates. Orthopaedics and Traumatology: Surgery and Research 96(4, Suppl.), S17–S36 (2010)
4. Dobbe, J., Strackee, S.D., Schreurs, A.W., Jonges, R., Carelsen, B., Vroemen, J., Grimbergen, C.A., Streekstra, G.J.: Computer-assisted planning and navigation for corrective distal radius osteotomy, based on pre- and intraoperative imaging. IEEE Trans. Biomed. Eng. 58(1), 182–190 (2011)
5. Dobbe, J., Vroemen, J.C., Strackee, S., Streekstra, G.: Patient-tailored plate for bone fixation and accurate 3d positioning in corrective osteotomy. Med. Biol. Eng. Comput. (2012) (in press)
6. Murase, T., Oka, K., Moritomo, H., Goto, A., Yoshikawa, H., Sugamoto, K.: Three-dimensional corrective osteotomy of malunited fractures of the upper extremity with use of a computer simulation system. The Journal of Bone and Joint Surgery 90(11), 2375–2389 (2008)
7. Cootes, T.F., Taylor, C.J., Cooper, D.H., Graham, J.: Active shape models - their training and application. Comp. Vis. and Im. Und. 61(1), 38–59 (1995)
8. van de Giessen, M., Foumani, M., Vos, F.M., Strackee, S.D., Maas, M., Vliet, L.V., Grimbergen, C.A., Streekstra, G.J.: A 4d statistical model of wrist bone motion patterns. IEEE Trans. Med. Imaging 31(3), 613–625 (2012)
9. Waarsing, J., Rozendaal, R., Verhaar, J., Bierma-Zeinstra, S., Weinans, H.: A statistical model of shape and density of the proximal femur in relation to radiological and clinical OA of the hip. Osteoarthritis and Cartilage 18(6), 787–794 (2010)
10. Chung, F., Schmid, J., Magnenat-Thalmann, N., Delingette, H.: Comparison of statistical models performance in case of segmentation using a small amount of training datasets. The Visual Computer 27(2), 141–151 (2011)
11. Schmid, J., Kim, J., Magnenat-Thalmann, N.: Robust statistical shape models for mri bone segmentation in presence of small field of view. Med. Im. Analys., 155–168 (2011)
12. Nicolella, D.P., Bredbenner, T.L.: Development of a parametric finite element model of the proximal femur using statistical shape and density modelling. Computer Methods in Biomechanics and Biomedical Engineering 15(2), 101–110 (2012)
13. Taylor, M., Bryan, R., Galloway, F.: Accounting for patient variability in finite element analysis of the intact and implanted hip and knee: a review. Int. J. Numer. Method Biomed. Eng. 29(2), 273–292 (2013)
14. Kozic, N., Weber, S., Büchler, P., Lutz, C., Reimers, N., Ballester, M.G., Reyes, M.: Optimisation of orthopaedic implant design using statistical shape space analysis based on level sets. Medical Image Analysis 14(3), 265–275 (2010)
15. Mahfouz, M., Fatah, E.E.A., Bowers, L.S., Scuderi, G.: Three-dimensional morphology of the knee reveals ethnic differences. Clin. Orthop. Relat. Res. 407(1), 172–185 (2012)
16. Whitmarsh, T., Fritscher, K.D., Humbert, L., del Río Barquero, L.M., Roth, T., Kammerlander, C., Blauth, M., Schubert, R., Frangi, A.F.: Hip fracture discrimination from dual-energy x-ray absorptiometry by statistical model registration. Bone 51(5), 896–901 (2012)

17. Baek, S.Y., Wang, J.H., Song, I., Lee, K., Lee, J., Koo, S.: Automated bone landmarks prediction on the femur using anatomical deformation technique. Computer-Aided Design 45(2), 505–510 (2013)
18. Johnson, A.E., Hebert, M.: Surface matching for object recognition in complex 3-d scenes. Image and Vision Computing 16, 635–651 (1998)
19. Wang, Y., Peterson, B.S., Staib, L.H.: 3d brain surface matching based on geodesics and local geometry. Comp. Vis. and Im. Under. 89(2-3), 252–271 (2003)
20. Feldmar, J., Malandain, G., Declerck, J., Ayache, N.: Extension of the icp algorithm to non-rigid intensity-based registration of 3d volumes. In: Proceedings of the IEEE Workshop on Mathematical Methods in Biomedical Image Analysis, vol. 14(2), pp. 84–93 (1996)
21. Caunce, A., Taylor, C.J.: Using local geometry to build 3d sulcal models. In: Kuba, A., Sámal, M., Todd-Pokropek, A. (eds.) IPMI 1999. LNCS, vol. 1613, pp. 196–209. Springer, Heidelberg (1999)
22. Fleute, M., Lavallée, S.: Building a complete surface model from sparse data using statistical shape models: Application to computer assisted knee surgery. In: Wells, W.M., Colchester, A.C.F., Delp, S.L. (eds.) MICCAI 1998. LNCS, vol. 1496, pp. 879–887. Springer, Heidelberg (1998)
23. Christensen, G.E., Rabbitt, R.D., Miller, M.I.: Deformable templates using large deformation kinematics. IEEE Transactions on Image Processing 5(10), 1435 (1996)
24. van de Giessen, M., Vos, F.M., Grimbergen, C.A., van Vliet, L.J., Streekstra, G.J.: An efficient and robust algorithm for parallel groupwise registration of bone surfaces. Med Image Comput Comput Assist Interv 15(3), 164–171 (2012)
25. Granger, S., Pennec, X.: Multi-scale EM-ICP: A fast and robust approach for surface registration. In: Heyden, A., Sparr, G., Nielsen, M., Johansen, P. (eds.) ECCV 2002, Part IV. LNCS, vol. 2353, pp. 418–432. Springer, Heidelberg (2002)
26. Vroemen, J., Dobbe, J., Jonges, R., Strackee, S., Streekstra, G.: Three-dimensional assessment of bilateral symmetry of the radius and ulna for planning corrective surgeries. J. Hand Surg. Am. 5(37), 982–988 (2012)
27. Dobbe, J., du Pré, K., Kloen, P., Blankevoort, L., Streekstra, G.: Computer-assisted and patient-specific 3-d planning and evaluation of a single-cut rotational osteotomy for complex long-bone deformities. Med. and Bio. Eng. and Comp. 49(12), 1363–1370 (2011)
28. Koenderink, J.J., van Doorn, A.J.: Surface shape and curvature scales. Im. and Vis. Computing 10(8), 557–564 (1992)